Published in final edited form as:
Nano Lett. 2013 December 11; 13(12): 6144–6150. doi:10.1021/nl403469r.

Nanopore-based identification of individual nucleotides for direct RNA sequencing

Mariam Ayub[1], **Steven W. Hardwick**[2], **Ben F. Luisi**[2], and **Hagan Bayley**[1,*]

[1]Department of Chemistry, University of Oxford, Oxford, OX1 3TA, UK

[2]Department of Biochemistry, University of Cambridge, Cambridge, CB2 1GA, UK

Abstract

We describe a label-free ribobase identification method, which uses ionic current measurement to resolve ribonucleoside monophosphates or diphosphates in α-hemolysin protein nanopores containing amino-cyclodextrin adapters. The accuracy of base identification is further investigated through the use of a guanidino-modified adapter. Based on these findings, an exosequencing approach is envisioned in which a processive exoribonuclease (polynucleotide phosphorylase) presents sequentially cleaved ribonucleoside diphosphates to a nanopore.

Keywords

α-hemolysin; nanopore; RNA sequencing; cyclodextrin; base identification; protein engineering

Single-molecule nanopore technology is being investigated as an ultra-rapid, low-cost platform for sequencing DNA and RNA molecules[1, 2]. Single-stranded DNA (ssDNA) is translocated through protein pores[3], such as the heptameric staphylococcal α-hemolysin (αHL) pore[4], and it was suggested that DNA sequence might be obtained from base-dependent transitions in the ionic current flowing through a pore[5]. Indeed, individual bases can be recognized by protein nanopores[6, 7]. Recently, advances in base recognition[8-11] and the use of enzymes that slowly ratchet DNA strands through pores to provide improved signal-to-noise[12-15] have culminated in the realization of nanopore sequencing in both the commercial arena[16-18] and in academia[19, 20]. In a second approach, exosequencing, bases are cleaved from a DNA strand by a processive exonuclease and identified as individual nucleotides by the nanopore[1, 7]. Excellent identification of nucleoside monophosphates has been obtained with engineered αHL pores carrying cyclodextrin adapters, which can be non-covalently bound within the pore[7] or covalently attached for continuous base identification[21].

*Corresponding Author: hagan.bayley@chem.ox.ac.uk.

Supporting Information: Details of experimental procedures, nucleoside monophosphate detection, oligonucleotide sequences, and the data displayed in Figures 1-5. This material is available free of charge via the Internet at http://pubs.acs.org.

Author Contributions: M.A., B.L. and H.B. conceived the ideas and designed the experiments. M.A. and S.H. performed the experiments. M.A. analyzed the data. M.A. and H.B. wrote the manuscript with contributions from all the authors. All authors have given approval to the final version of the manuscript.

The authors declare no competing financial interest.

Notes: Hagan Bayley is the Founder, a Director and a share-holder of Oxford Nanopore Technologies, a company engaged in the development of nanopore sequencing technology. Work in the Bayley laboratory at the University of Oxford, including this work, is supported in part by Oxford Nanopore Technologies.

However, for both strand sequencing and exosequencing the focus has remained primarily on DNA, with RNA sequencing receiving less attention. The ability to obtain ultra-rapid RNA sequence information with nanopores would be of considerable significance. For example, it would allow the estimation of mRNA levels in cells and reveal splice patterns and other post-transcriptional modifications[22-24], including potential covalent modifications that may have regulatory consequence. Such measurements will be invaluable as a tool for discovery and in medical diagnostics[23, 25-27]. Nanopore RNA sequencing might also be used to identify and estimate the abundance of small regulatory RNAs, such as bacterial sRNA and eukaryotic miRNA[28-30].

Short ssRNA homopolymer molecules have been identified based on differences in residual current (I_{RES}) recorded while the RNAs are translocating through the αHL pore[5, 31]. The transition between two homopolymer sequences poly(rA) and poly(rC) within a single translocating RNA molecule have also been observed based upon small differences in the polymer's helical structures[31]. We have demonstrated that individual bases in immobilized ssRNA can be distinguished based on ionic current flow[32]. By using the αHL NNY pore, which has superior nucleobase discrimination properties, we could distinguish between the standard bases (rG, rA, rC, and rU) and the modified bases rI, m^6A and m^5C. We have also shown that long ssRNAs of up to 6 kb can be translocated through an αHL pore in an applied potential[33].

In the present paper, we lay the groundwork for RNA exosequencing by showing that ribonucleoside diphosphates (rNDPs) can be detected and distinguished by using engineered αHL pores containing cyclodextrin adapters within the transmembrane β barrel (Figure 1). We propose to use polynucleotide phosphorylase (PNPase), which processively cleaves ssRNA in the 3′-to-5′ direction using inorganic phosphate (P_i) to attack the phosphoester linkage and liberate rNDPs. Sequencing approaches, such as this, which distinguish natural nucleobases are advantageous[1, 2] and the additional charge on rNDPs (over NMPs)[7, 21] is likely to result in more efficient capture by the nanopore.

Detection of rNDPs with non-covalently-attached cyclodextrin adapters

We used the M113R-RL2 mutant of αHL[34] (Figures S1). M113R αHL pores have previously been shown to bind cyclodextrin (CD) adapters[35], which in turn bind NMPs allowing their identification by current recording[7, 21]. Following the earlier work, we used β-cyclodextrin with the seven primary hydroxyls replaced with amino groups (heptakis-(6-deoxy-6-amino)-β-cyclodextrin; hereafter referred to as am_7βCD) (Figure S2). Because am_7βCD is added to the trans compartment, the positively charged amino groups promote an extended residence time for the CD at positive applied potentials, which is long compared to the residence times of the nucleotides[7, 21]. We have proposed that the Arg residues at position 113 interact with nucleobase rings, while the amino groups on the cyclodextrin ring interact with phosphate groups[7]. By using this approach in the present study, all four standard ribonucleoside monophosphates (rGMP, rAMP, rUMP, rCMP) could be distinguished (Table S1). Here, we focus on the ribonucleoside diphosphates rGDP, rADP, rUDP and rCDP.

In the absence of am_7βCD, the M113R-RL2 pore (Figure S3) remained open and passed a current $I_O^{M113R\text{-}RL2}$ = 123.0 ± 4.0 pA (n = 47, independent experiments) at +120 mV in 10 mM Tris-HCl, 1.2 M KCl, at pH 6.0. The addition of 80 μM am_7βCD to the trans compartment produced reversible blocking events (Figure S4, Table S2) with a residual current level $I_{RES\text{-}am7\beta CD}$ = 59.0 ± 2.0 pA (n = 47) (Figure 2a, top panel). Upon the sequential addition of rNDPs (10 μM rADP; 10 μM rUDP; 10 μM rCDP; 10 μM rGDP) to the cis compartment, additional current blockades were observed originating from the CD-

blocked level (Figure 2a, bottom panel). These represent the binding of rNDPs to am$_7$βCD lodged within the M113R-RL2 pore.

The blockades were plotted as $I_{RES\%}$ histograms (Figure 2b, $I_{RES\%} = (I_{RES}/I_O) \times 100$)). rUDP blocked the pore to the highest extent ($I_{RES\%}^{rUDP} = 20.7 \pm 0.8\%$), followed by rADP ($I_{RES\%}^{rADP} = 21.9 \pm 0.3\%$), rGDP ($I_{RES\%}^{rGDP} = 23.1 \pm 0.7\%$) and rCDP ($I_{RES\%}^{rCDP} = 24.1 \pm 0.7\%$). The difference in residual current between the two most widely dispersed current peaks in the histogram was $\Delta I_{RES\%}^{OVERALL} = 3.4 \pm 0.3\%$ (n = 47) (Table S3). The products of the sequential differences (δ) between each of the four residual current levels in the histograms were also used to measure the ability of different pores to discriminate between the four nucleotide. An αHL pore that is unable to discriminate between all rNDPs has δ = 0 (i.e. the current levels of two or more rNDPs overlap). For the experiment shown in Figure 2b, $\delta^{M113R\text{-}RL2} = 1.4 \pm 0.6$ at +120 mV.

The rNDPs also showed variations in mean dwell time (τ_{off}) within the CD adapter (Table S3). Longer binding events are desirable for accurate base calling as they allow a better estimate of the residual pore current. However, higher τ_{off} values would decrease the overall rate of sequencing. For the accurate sequential reading of nucleotides, the rNDP must exit the nanopore on the trans side of the bilayer to remove the possibility of the nucleotide being re-read. The variation in the dissociation rate constant k_{off} ($1/\tau_{off}$) with the applied potential can be used to determine whether a bound molecule exits a nanopore on the cis or trans side of the bilayer[21, 36, 37]. Therefore, the voltage dependences of the k_{off} values for rNDPs bound to the am$_7$βCD adapter were determined (Figure 2d, Figure S5 and Table S4). At low potentials, under which the nucleotide returns to the cis compartment, we observed high k_{off} values for the four rNDPs (+100 mV; k_{off} = 40 to 54 s^{-1}) (Figure 2d). Higher potentials promoted the binding of the charged nucleotides to the cyclodextrin adapter, resulting in a decrease in k_{off} (at +180 mV; k_{off}= 32 to 45 s^{-1}). At high potential, k_{off} increases for nucleotides rCDP and rUDP suggesting their translocation through the pore. However, higher potential may be required for complete translocation of all four rNDPs.

The discrimination of rGDP rADP, rUDP and rCDP was compared over a range of physical conditions. The KCl concentration was varied from 500 mM to 1.2 M and the pH value over the range pH = 6.0 to 8.0. The applied potential was also adjusted to fine tune the separation of the peaks in the $I_{RES\%}$ histogram. First, we found that high concentrations of KCl (1 M and 1.2 M) gave the best discrimination (1 M, $\Delta I_{RES\%}^{OVERALL} = 3.1 \pm 0.5\%$ (n = 40); 1.2 M, $\Delta I_{RES\%}^{OVERALL} = 3.4 \pm 0.3\%$ (n = 47) compared with 500 mM KCl ($\Delta I_{RES\%}^{OVERALL} = 1.7 \pm 0.4\%$ (n = 9)). Second, the residual current levels were pH dependent. Tris-HCl buffers containing 1.2 M KCl at pH values of 6.0, 7.0, 7.5 and 8.0 were examined. Between pH 7.0 and 8.0, only three current levels were observed when the rNDPs bound to am$_7$βCD lodged within the M113R-RL2 pore (Figure S6). At pH 6.0, all four rNDPs could be distinguished (Figure 2, Figure S6). Third, nucleotide binding was voltage dependent. At +100 mV, very few binding events were observed, suggesting that a minimum potential is required to drive the rNDPs into the CD binding site (Figure S5 and Table S4), whereas higher potentials (> +160 mV) resulted in a two-fold increase in the frequency of binding events. However, at +200 mV, the $I_{RES\%}$ levels were too close to each other to allow the rNDPs to be distinguished (Figure 2c). $\Delta I_{RES\%}^{OVERALL} = 2.3 \pm 0.8\%$; (n = 41), hence, the optimal base discrimination was recorded within a window of +120 to +140 mV.

Two additional M113X-RL2 pores were also investigated[35, 38]: M113N-RL2 and M113F-RL2 (Table S2, Figure S3). Under the conditions described above (buffer: 10 mM Tris-HCl, 1.2 M KCl, at pH 6.0) M113N-RL2 bound am$_7$βCD, but individual rNDPs could not be distinguished, because of an increase in the overlap between the blockade levels: $\Delta I_{RES\%}^{OVERALL} = 1.1 \pm 0.6\%$; (n = 6); $\delta^{M113N\text{-}RL2} = 0.2 \pm 0.1$. M113F-RL2 gave results

similar to M113R-RL2, but the peak separations between the rNDPs were smaller: $\Delta I_{RES\%}{}^{OVERALL} = 2.4 \pm 0.6\%$; (n = 9); $\delta^{M113F\text{-}RL2} = 0.9 \pm 0.4$. In fact, the original mutant, αHL M113R-RL2 displayed the best discrimination with $\delta^{M113R\text{-}RL2} = 1.4 \pm 0.6$ at +120 mV.

An alternative non-covalent adapter

In addition to the am_7βCD adapter, heptakis(6-deoxy-6-guanidino)-βCD (gu_7βCD)[39] was tested for rNDP discrimination. The molecule comprises βCD with seven guanidinium groups in place of the primary hydroxyls (Figure 2e-f), with the guanidinium groups having a higher pKa values than the primary amines in am_7βCD. We built a speculative model of the complex that is formed between rGDP and gu_7βCD using ChemBioDraw software (version 12.02), compatible with Y. Astier's proposed model[7]. Here the rGDP molecule binds to the gu_7βCD by locating its ionic phosphates close to the guanidinium residues while allowing the guanine moiety to penetrate the CD cavity (Figure 2f). At +120 mV, we observed comparable dispersion of the peaks in the $I_{RES\%}$ histogram when gu_7βCD (80 μM, trans) was used: $\Delta I_{RES\%}{}^{OVERALL} = 4.3 \pm 0.4\%$ (n = 31), compared to $\Delta I_{RES\%}{}^{OVERALL} = 3.4 \pm 0.3\%$ (n = 47) for am_7βCD under the same optimal experimental conditions (1.2 M KCl, 10 mM Tris-HCl, at pH 6.0) Figure 2g, Table S5). The mean dwell times for rNDP (τ_{off}) with gu_7βCD (11 to 21 ms) were similar to those with am_7βCD (9 to 20 ms) (Figure 2h, Table S5), with rGDP giving the largest difference: $\tau_{off}{}^{rGDP}$ (gu_7βCD = 16.0 ± 1.0 ms (n = 31); $\tau_{off}{}^{rGDP}$ (gu_7βCD = 16.0 ± 1.0 ms (n = 31); $\tau_{off}{}^{rGDP}$ (am_7βCD = 11.0 ± 1.0 ms (n = 47) (Table 1).

Continuous detection of rNDPs by using a permanent cyclodextrin adapter

For sequencing applications, a permanent adapter would be desirable for continuous base detection. We have shown that CDs can be covalently attached within the αHL pore[40] and used to distinguish dNMPs[21]. Hence, the αHL-$(N139Q)_6(N139Q/L135C)_1$.am_6-$amPDP_1$-βCD pore[21] was tested for its ability to discriminate between the four rNDPs (Figure 3a, Figure S7). This αHL-$(N139Q)_6(N139Q/L135C)_1$.am_6-$amPDP_1$-βCD pore was constructed from a reactive cyclodextrin: heptakis(6-deoxy-6-amino)-6-N-mono(2-pyridyl)dithiopropanoyl-β-cyclodextrin (am_6am-PDP_1βCD) which contains six primary amino groups required for base detection and a reactive linker for covalent attachment to the cysteine residue (at position L135) within the barrel of the αHL $(N139Q)_6(N139Q/L135C)_1$ pore. At a potential of +160 mV, the current passed by αHL-$(N139Q)_6$($N139Q/L135C)_1$.am_6-$amPDP_1$-βCD was recorded (Figure 3b, top panel), and then rGDP, rADP, rUDP and rCDP were sequentially added to the cis compartment (Figure 3b, bottom panel) and an $I_{RES\%}$ histogram was compiled from the recording (Figure 3c). In 1 M KCl, 25 mM Tris-HCl, at pH 7.5, rGDP showed the largest block ($I_{RES\%}{}^{rGDP} = 27.7 \pm 0.2\%$), followed by rADP ($I_{RES\%}{}^{rADP} = 29.5 \pm 0.3\%$), rCDP ($I_{RES\%}{}^{rCDP} = 31.8 \pm 0.3\%$) and rUDP ($I_{RES\%}{}^{rUDP} = 32.4 \pm 0.3\%$). At lower potentials (+120 mV), rCDP and rUDP showed good separation, but the peaks for rGDP and rADP overlapped. The optimal potential was between +160 and +180 mV (Figure 3e). The outcome was comparable with the non-covalently attached am_7βCD $\Delta I_{RES\%}{}^{OVERALL} = 4.7 \pm 0.3\%$ (n = 22) with $\delta = 3.1 \pm 1.0$ (Table 1, Table S6) with the additional advantage that rNDPs are read continuously.

The rNDPs also showed variations in mean dwell time (τ_{off}) within the αHL-$(N139Q)_6(N139Q/L135C)_1$.am_6-$amPDP_1$-βCD pore, with τ_{off} values in the range 18 to 26 ms, rGDP having the longest dwell time: $\tau_{off}{}^{rGDP} = 26.0 \pm 2.0$ %, at +160 mV (Figure 3d, Table 1, Tables S6 and S7). The variations in k_{off} ($1/\tau_{off}$) with the applied potential for the αHL-$(N139Q)_6(N139Q/L135C)_1$.am_6-$amPDP_1$-βCD pore were similar to the relationships obtained with non-covalently attached am_7βCD (Figure 3d). An increase in k_{off} at higher

potentials (> +160 mV) was seen for all four rNDPs, indicating that these nucleotides cross into the trans compartment. The optimal base discrimination was obtained between +160 mV and +180 mV, potentials at which a high proportion of rNDPs translocate through the nanopore: at +180 mV with αHL-$(N139Q)_6(N139Q/L135C)_1$.am_6-$amPDP_1$-βCD, τ_{off}^{rGDP} = 25.0 ± 1.0 ms; τ_{off}^{rADP} = 21.0 ± 1.0 ms; τ_{off}^{rCDP} = 22.0 ± 1.0 ms; τ_{off}^{rUDP} = 17.0 ± 1.0 ms (n = 22). Future work on this can include testing the guanidinium-cyclodextrin (gu_7βCD), which may also be attached using a similar strategy, to provide continuous read of nucleotides and improved accuracy of the residual current measured.

Detection of rNDP derived from ssRNA

We also used the M113R-RL2 αHL pore with am_7βCD to identify rNDPs generated in situ from ssRNA by using the RNA-selective enzyme polynucleotide phosphorylase (PNPase) from *Caulobacter crescentus*[41, 42] (Figure 4a, Figure S8). To ensure that the conditions for nucleotide discrimination were compatible with PNPase activity[41], we maintained pH asymmetry: pH (cis) = 7.0 (to promote enzyme activity); pH (trans) = 6.0 (to maintain nucleotide discrimination). Two samples of RNA were used: one contained three homopolymers: oligo(rC)$_{30}$, oligo(rU)$_{30}$, oligo(rA)$_{30}$ and the second, a heteropolymer, oligo(het)$_{30}$, with all four ribobases rG, rC, rU and rA: 3′-AAAUGGACUGGCUUCGGAAGCCAAAUGGAU-5′ (Table S8). Upon the addition of PNPase and the ssRNA molecules to the cis compartment (in the absence of P_i and Mg^{2+} and am_7βCD) a decrease in the ionic current through the nanopore from the open state level can occur when (i) ssRNA is freely translocating through the pore or (ii) the PNPase•RNA complex is captured (Figure 4a). The enzyme is too large to enter the nanopore and holds the 3′-end of the RNA substrate at the cis entrance. In this state, the ssRNA that has entered the pore causes a sequence-dependent decrease in the ionic current, but is not translocated into the trans compartment.

We recorded current blocks for the capture of PNPase-bound oligo(rA)$_{30}$, oligo(rC)$_{30}$ and oligo(rU)$_{30}$ at +140 mV (Figure 4b, Figures S9, S10 and Table S9), and compiled the corresponding $I_{RES\%}$ histograms (Figure 4c). PNPase-bound oligo(rU)$_{30}$ blocked the pore to a greater extent ($I_{RES\%}^{oligo(rU)}$ = 22.2 ± 0.2%) than oligo(rA)$_{30}$ ($I_{RES\%}^{oligo(rA)}$ = 24.3 ± 0.2%) and oligo(rC)$_{30}$ ($I_{RES\%}^{oligo(rC)}$ = 26.6 ± 0.2%). After the addition of 5 mM Mg^{2+} and 10 mM P_i (10 mM NaH_2PO_4, pH 7.0) to the cis compartment (Figure 4a), the PNPase was activated and sequentially cleaved rNDPs from the 3′-end of the ssRNA. The liberated rNDPs were observed as binding events when am_7βCD was added to the trans compartment. As expected, we observed three peaks corresponding to the three released rNDPs (Figure 4d): $I_{RES\%}^{rUDP}$ = 26.9 ± 0.7% < $I_{RES\%}^{rADP}$=28.8 ± 0.9% < $I_{RES\%}^{rCDP}$= 31.3 ± 0.6% with $\Delta I_{RES\%}^{OVERALL}$ = 4.4 ± 0.8% and $\delta^{M113R\text{-}RL2}$= 4.7 ± 0.8 (n = 8), (Table S9).

To test the ability of the nanopore to identify all four nucleosides diphosphates, oligo(het)$_{30}$ was used. Oligo(het)$_{30}$ bound to the PNPase was captured by the M113R-RL2 pore at +140 mV, giving a single peak in the residual current histogram ($I_{RES\%}^{oligo(het)30}$ = 25.2 % ± 0.4%, Figure 4e, Table S10). Upon the addition of Mg^{2+} and P_i to cis, and subsequently am_7βCD, to the trans compartment, the rNDPs were readily distinguished by their residual currents: $I_{RES\%}^{rUDP}$ = 25.8 ± 0.6% < $I_{RES\%}^{rADP}$ = 27.1 ± 0.6% < $I_{RES\%}^{rGDP}$ = 28.2 ± 0.9% < $I_{RES\%}^{rCDP}$ = 29.9 ± 0.6%; $\Delta I_{RES\%}^{OVERALL}$ = 4.1 ± 0.8 %; $\delta^{M113R\text{-}RL2}$= 2.4 ± 0.7 (n = 5) (Figure 4f and Figure S11, Table S10). The mean dwell times were τ_{off}^{rGDP}=25.0±2.0 ms, τ_{off}^{rADP} = 19.0 ± 1.0 ms,τ_{off}^{rCDP} = 21.0 ± 1.0 ms, τ_{off}^{rUDP} = 17.0 ± 1.0 ms (n = 5) (Table S10). These experiments support our findings with the free nucleotides and the am_7βCD cyclodextrin adapter (Figure 2). The nucleotides released by PNPase give similar $I_{RES\ \%}$ and τ_{off} values (at a potential of +120 mV). Therefore, it should be possible to integrate PNPase

with the αHL pore to distinguish individual nucleotides released from a ssRNA under conditions compatible with enzyme activity.

Monitoring PNPase digestion of ssRNA

The 3′-phosphorolytic activity of PNPase is dependent upon inorganic phosphate (P_i), which attacks the phosphodiester bond of ssRNA. Nanopore experiments reported this catalytic activity as an abrupt decrease in translocation-event frequency after the addition of 10 mM P_i to the cis compartment in the presence of PNPase•oligo-[P](het$_{30}$) (Figure 5a,b, Table S11). In contrast, the translocation-event frequency for an oligonucleotide with a phosphorothioate backbone, oligo-[PS](het)$_{30}$, which cannot be cleaved by PNPase[43-45]; remains unchanged after P_i addition (Figure 5b). The time course of ssRNA digestion by PNPase was determined by nanopore analysis (Figure 5c, Table S12) yielding $K_m = 0.4 \pm 0.1$ mM (derived from a Lineweaver-Burk plot) consistent with previously reported biochemical studies conducted in bulk solution[41, 42, 46-50]. These measurements reveal important details of PNPase kinetics which may be useful for the alignment of the ssRNA-PNPase catalytic process and the subsequent detection using the cyclodextrin adapter.

Conclusions

We have shown that engineered αHL nanopores with either non-covalently bound or covalently attached CD adapters accurately discriminate between the four standard rNMPs and rNDPs under optimized experimental conditions. Pores with covalently attached CD adapters are capable of continuous nucleotide detection. In addition, our platform operates under conditions compatible with PNPase activity. While many enzymes that handle nucleic acids prefer low salt conditions, PNPase is active at high KCl concentrations, allowing data acquisition under conditions suited for optimal nucleotide discrimination. The results presented here offer the groundwork to develop a platform suitable for RNA nanopore exosequencing. For high-throughput parallel analysis, thousands of pores must be integrated into arrays and feasible strategies toward this end are currently under investigation[16, 51].

Supplementary Material

Refer to Web version on PubMed Central for supplementary material.

Acknowledgments

This work was supported by grants from the National Institutes of Health, Wellcome Trust and Oxford Nanopore Technologies. BFL and SWH are supported by the Wellcome Trust. The authors thank Oxford Nanopore Technologies for the αHL-(N139Q)$_6$(N139Q/L135C)$_1$.am$_6$-amPDP$_1$-βCD protein and gu$_7$βCD, Ellina Mikhailova for the M113X-RL2 mutants and James Clarke and Lakmal Jayasinghe for valuable discussions.

References

1. Bayley H. Current Opinion in Chemical Biology. 2006; 10(6):628–637. [PubMed: 17113816]
2. Branton D, Deamer DW, Marziali A, Bayley H, Benner SA, Butler T, Di Ventra M, Garaj S, Hibbs A, Huang X, Jovanovich SB, Krstic PS, Lindsay S, Ling XS, Mastrangelo CH, Meller A, Oliver JS, Pershin YV, Ramsey JM, Riehn R, Soni GV, Tabard-Cossa V, Wanunu M, Wiggin M, Schloss JA. Nat Biotech. 2008; 26(10):1146–1153.
3. Muthukumar M. Annual Review of Biophysics and Biomolecular Structure. 2007; 36(1):435–450.
4. Song LZ, Hobaugh MR, Shustak C, Cheley S, Bayley H, Gouaux JE. Science. 1996; 274(5294): 1859–1866. [PubMed: 8943190]
5. Kasianowicz JJ, Brandin E, Branton D, Deamer DW. Proc Natl Acad Sci U S A. 1996; 93(24): 13770–3. [PubMed: 8943010]

6. Ashkenasy N, Sánchez-Quesada J, Bayley H, Ghadiri MR. Angewandte Chemie International Edition. 2005; 44(9):1401–1404.
7. Astier Y, Braha O, Bayley H. Journal of the American Chemical Society. 2006; 128(5):1705–1710. [PubMed: 16448145]
8. Stoddart D, Heron AJ, Mikhailova E, Maglia G, Bayley H. Proc Natl Acad Sci U S A. 2009; 106(19):7702–7. [PubMed: 19380741]
9. Purnell RF, Schmidt JJ. ACS Nano. 2009; 3(9):2533–8. [PubMed: 19694456]
10. Derrington IM, Butler TZ, Collins MD, Manrao E, Pavlenok M, Niederweis M, Gundlach JH. Proceedings of the National Academy of Sciences. 2010
11. Manrao EA, Derrington IM, Pavlenok M, Niederweis M, Gundlach JH. PLoS One. 2011; 6(10):e25723. [PubMed: 21991340]
12. Cockroft SL, Chu J, Amorin M, Ghadiri MR. Journal of the American Chemical Society. 2008; 130(3):818–820. [PubMed: 18166054]
13. Olasagasti F, Lieberman KR, Benner S, Cherf GM, Dahl JM, Deamer DW, Akeson M. Nat Nanotechnol. 2010; 5(11):798–806. [PubMed: 20871614]
14. Chu J, Gonzalez-Lopez M, Cockroft SL, Amorin M, Ghadiri MR. Angew Chem Int Ed Engl. 2010; 49(52):10106–9. [PubMed: 21105031]
15. Lieberman KR, Cherf GM, Doody MJ, Olasagasti F, Kolodji Y, Akeson M. J Am Chem Soc. 2010; 132(50):17961–72. [PubMed: 21121604]
16. Pennisi E. Science. 2012; 336(6081):534–537. [PubMed: 22556226]
17. Schneider GF, Dekker C. Nat Biotech. 2012; 30(4):326–328.
18. Bayley H. Physics of Life Reviews. 2012; 9(2):161–163. [PubMed: 22652072]
19. Cherf GM, Lieberman KR, Rashid H, Lam CE, Karplus K, Akeson M. Nat Biotechnol. 2012; 30(4):344–8. [PubMed: 22334048]
20. Manrao EA, Derrington IM, Laszlo AH, Langford KW, Hopper MK, Gillgren N, Pavlenok M, Niederweis M, Gundlach JH. Nat Biotechnol. 2012; 30(4):349–53. [PubMed: 22446694]
21. Clarke J, Wu HC, Jayasinghe L, Patel A, Reid S, Bayley H. Nat Nano. 2009; 4(4):265–270.
22. Wang Z, Gerstein M, Snyder M. Nat Rev Genet. 2009; 10(1):57–63. [PubMed: 19015660]
23. Marguerat S, Wilhelm BT, Bahler J. Biochem Soc T. 2008; 36:1091–1096.
24. Mortazavi A, Williams BA, McCue K, Schaeffer L, Wold B. Nat Meth. 2008; 5(7):621–628.
25. Maher CA, Kumar-Sinha C, Cao X, Kalyana-Sundaram S, Han B, Jing X, Sam L, Barrette T, Palanisamy N, Chinnaiyan AM. Nature. 2009; 458(7234):97–101. [PubMed: 19136943]
26. Maher B. Nature. 2009; 459(7244):146–7. [PubMed: 19444175]
27. Wanunu M, Bhattacharya S, Xie Y, Tor Y, Aksimentiev A, Drndic M. ACS Nano. 2011; 5(12): 9345–9353. [PubMed: 22067050]
28. Carthew RW, Sontheimer EJ. Cell. 2009; 136(4):642–655. [PubMed: 19239886]
29. Wanunu M, Dadosh T, Ray V, Jin J, McReynolds L, Drndic M. Nat Nano. 2010; 5(11):807–814.
30. Wang Y, Zheng D, Tan Q, Wang MX, Gu LQ. Nat Nano. 2011; 6(10):668–674.
31. Akeson M, Branton D, Kasianowicz JJ, Brandin E, Deamer DW. Biophys J. 1999; 77(6):3227–33. [PubMed: 10585944]
32. Ayub M, Bayley H. Nano Lett. 2012; 12(11):5637–5643. [PubMed: 23043363]
33. Cracknell JA, Japrung D, Bayley H. Nano Lett. 2013; 13(6):2500–2505. [PubMed: 23678965]
34. Cheley S, Gu LQ, Bayley H. Chemistry & biology. 2002; 9(7):829–838. [PubMed: 12144927]
35. Banerjee A, Mikhailova E, Cheley S, Gu LQ, Montoya M, Nagaoka Y, Gouaux E, Bayley H. Proceedings of the National Academy of Sciences. 2010; 107(18):8165–8170.
36. Sanchez-Quesada J, Ghadiri MR, Bayley H, Braha O. Journal of the American Chemical Society. 2000; 122(48):11757–11766.
37. Gu LQ, Cheley S, Bayley H. Science. 2001; 291(5504):636–640. [PubMed: 11158673]
38. Gu LQ, Cheley S, Bayley H. The Journal of General Physiology. 2001; 118(5):481–494. [PubMed: 11696607]

39. Yuan DQ, Izuka A, Fukudome M, Rekharsky MV, Inoue Y, Fujita K. Tetrahedron Letters. 2007; 48(19):3479–3483.
40. Wu HC, Astier Y, Maglia G, Mikhailova E, Bayley H. Journal of the American Chemical Society. 2007; 129(51):16142–16148. [PubMed: 18047341]
41. Hardwick SW, Gubbey T, Hug I, Jenal U, Luisi BF. Open Biology. 2012; 2(4)
42. Hardwick SW, Chan VSY, Broadhurst RW, Luisi BF. Nucleic Acids Research. 2011; 39(4):1449–1459. [PubMed: 20952404]
43. Eckstein F. Annu Rev Biochem. 1985; 54:367–402. [PubMed: 2411211]
44. Eckstein F, Gindl H. European Journal of Biochemistry. 1970; 13(3):558–564. [PubMed: 5444162]
45. Hornblower B, Coombs A, Whitaker RD, Kolomeisky A, Picone SJ, Meller A, Akeson M. Nat Meth. 2007; 4(4):315–317.
46. Nurmohamed S, Vincent HA, Titman CM, Chandran V, Pears MR, Du D, Griffin JL, Callaghan AJ, Luisi BF. J Biol Chem. 2011; 286(16):14315–14323. [PubMed: 21324911]
47. Godefroy T. European Journal of Biochemistry. 1970; 14(2):222–231. [PubMed: 4918555]
48. Chou JY, Singer MF. J Biol Chem. 1970; 245(5):995-&. [PubMed: 4313707]
49. Chou JY, Singer MF, Mcphie P. J Biol Chem. 1975; 250(2):508–514. [PubMed: 1078670]
50. Chang SA, Cozad M, Mackie GA, Jones GH. Journal of Bacteriology. 2008; 190(1):98–106. [PubMed: 17965156]
51. Hall AR, Scott A, Rotem D, Mehta KK, Bayley H, Dekker C. Nat Nanotechnol. 2010; 5(12):874–7. [PubMed: 21113160]

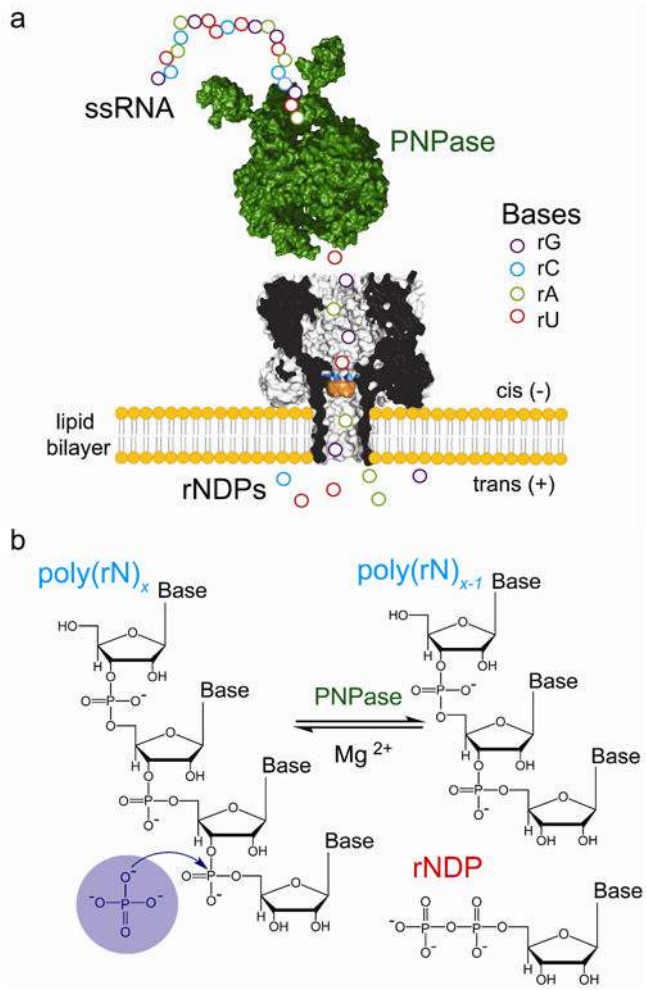

Figure 1.

Detection of nucleotides cleaved from ssRNA by polynucleotide phosphorylase. (a) Schematic representation of a ssRNA oligonucleotide (circles) digested by polynucleotide phosphorylase (PNPase, green), one base at a time. The liberated nucleotides (rNDPs) are detected by the heptameric αHL pore (7AHL) equipped with a cyclodextrin adapter ($am_7\beta CD$, orange). The mutant M113R (mutation highlighted in blue) was used in most of the experiments reported in this paper. In a functioning nanopore sequencer, the PNPase would be covalently attached to the αHL pore. (b) PNPase processively cleaves ssRNA substrates in the 3′-to-5′ direction by using inorganic phosphate (P_i) to attack the phosphodiester linkage nearest the 3′ terminus to release rNDPs.

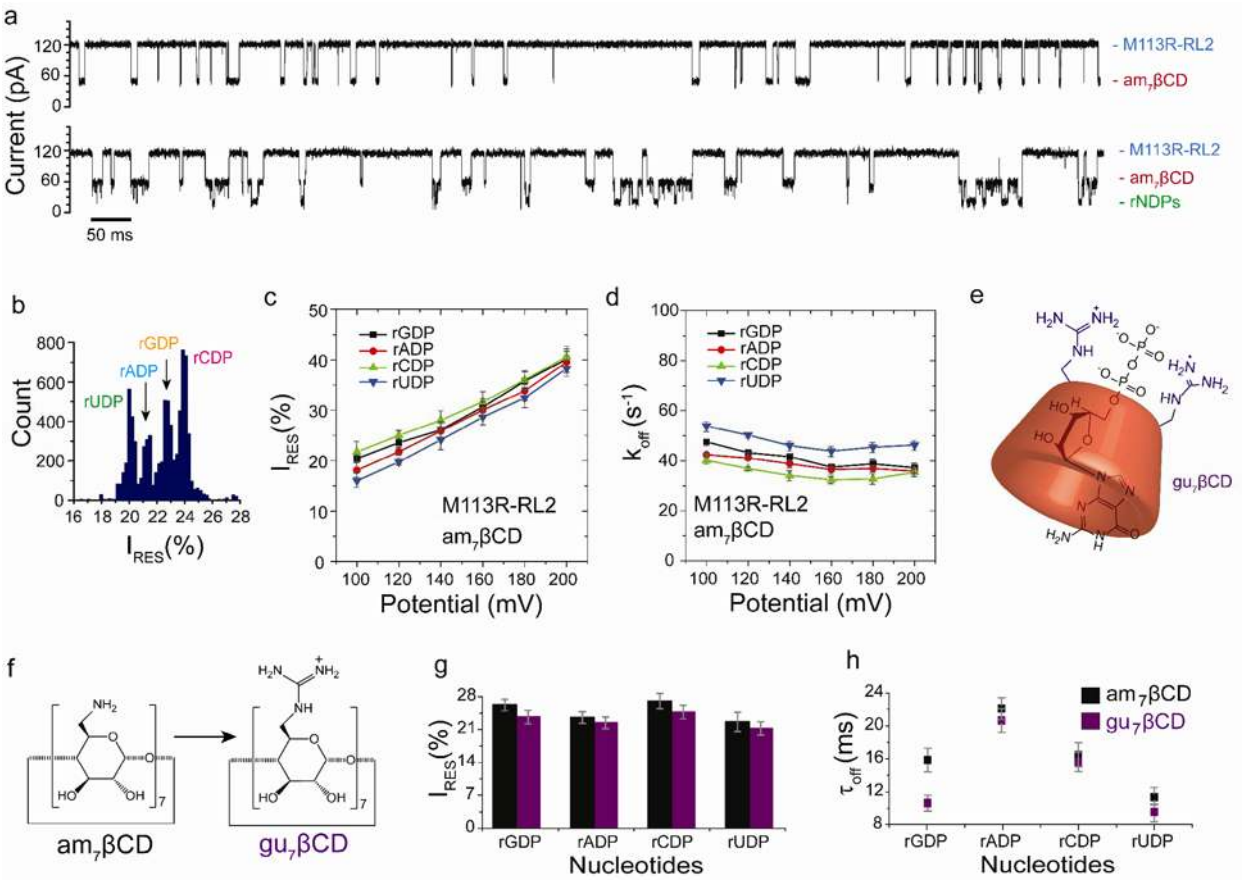

Figure 2.

Nucleoside diphosphate discrimination with non-covalently attached cyclodextrin adapters. (a) Single-channel recordings from the homoheptameric αHL M113R-RL2 pore showing am$_7$βCD binding (top) and rNDP detection with the am$_7$βCD adapter (bottom). (b) Corresponding residual current ($I_{RES\%}$) histogram. Data were acquired in 1.2 M KCl, 25 mM Tris-HCl, pH 6.0, at +120 mV in the presence of 80 μM am$_7$βCD (trans), 10 μM rGDP, 10 μM rADP, 10 μM rCDP and 10 μM rUDP (all cis). The results displayed are from a typical experiment. (c) Variation of residual currents ($I_{RES\%}$) with applied potential for each rNDP detected with the M1 13R-RL2•am$_7$βCD pore. (d) Variation of k_{off} with applied potential for each rNDP detected with the M1 13R-RL2•$_7$βCD pore. Values of k_{off} were determined by using $k_{off} = 1/\tau_{off}$, where τ_{off} is the mean dwell time for each rNDP in the pore. (e) Schematic representation of the complex of rGDP with gu$_7$βCD, created using ChemBioDraw software (version 12.02). (f) Conversion of am$_7$βCD to gu$_7$βCD[39]. For clarity, only two of the seven guanidino groups are shown. (g) Comparison of residual currents ($I_{RES\%}$) for each rNDP detected with the am$_7$βCD and gu$_7$βCD cyclodextrins within the αHL M113R-RL2 pore (n = 22). (h) mean dwell times (τ_{off}) for each rNDP detected with the am$_7$βCD and gu$_7$βCD cyclodextrins within the αHL M113R-RL2 pore (n = 22).

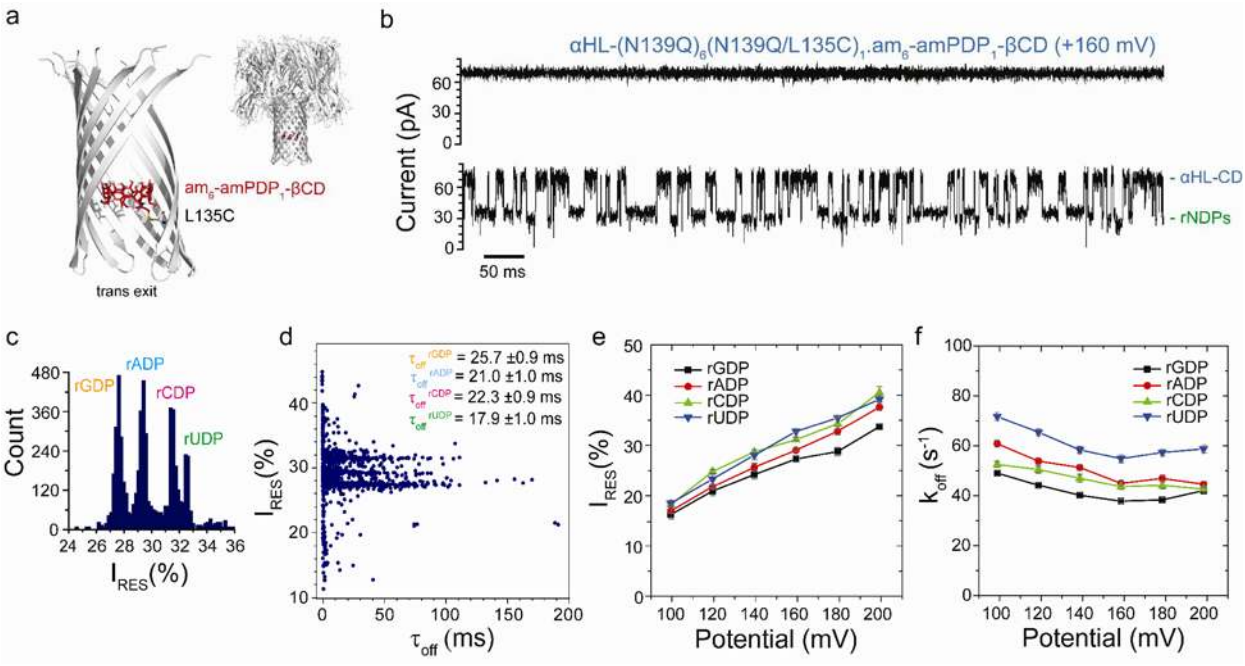

Figure 3.

rNDP interaction with the αHL-$(N139Q)_6(N139Q/L135C)_1.am_6$-$amPDP_1$-βCD pore. (a) Structure of the αHL-$(N139Q)_6(N139Q/L135C)_1.am_6$-$amPDP_1$- βCD pore (cartoon view). The enlarged view shows a close-up of the β barrel with two subunits omitted. The cyclodextrin (am_6-$amPDP_1$-βCD) was covalently attached through a disulfide bond to position 135 in one of the seven subunits, which had been mutated to Cys (red, sticks model)[21](b) Single-channel recording from the αHL-$(N139Q)_6(N139Q/L135C)_1.am_6$-$amPDP_1$-βCD pore showing continuous rNDP detection. (c) Corresponding residual current ($I_{RES\%}$) histogram. Data were acquired in 1 M KCl, 25 mM Tris-HCl, pH 7.5, at +160 mV in the presence of 10 μM rGDP, 10 μM rADP, 10 μM rCDP and 10 μM rUDP (all cis). The results displayed are from a typical experiment. (d) Scatter plot showing $I_{RES\%}$ and dwell times (τ_{off}) for rNDP binding events to the αHL-$(N139Q)_6(N139Q/L135C)_1.am_6$-$amPDP_1$-βCD pore as seen in the current trace in 'b'. (e) Variation of residual currents ($I_{RES\%}$) with applied potential for each rNDP detected with the αHL-$(N139Q)_6(N139Q/L135C)_1.am_6$-$amPDP_1$βCD pore. (f) Variation of k Values of k_{off} with applied potential for each rNDP detected with the αHL-$(N139Q)_6(N139Q/L135C)_1.am_6$-$amPDP_1$-βCD pore. Values of k_{off} were determined by using $k_{off} = 1/\tau_{off}$ where τ_{off} is the mean dwell time of the rNDP in the pore.

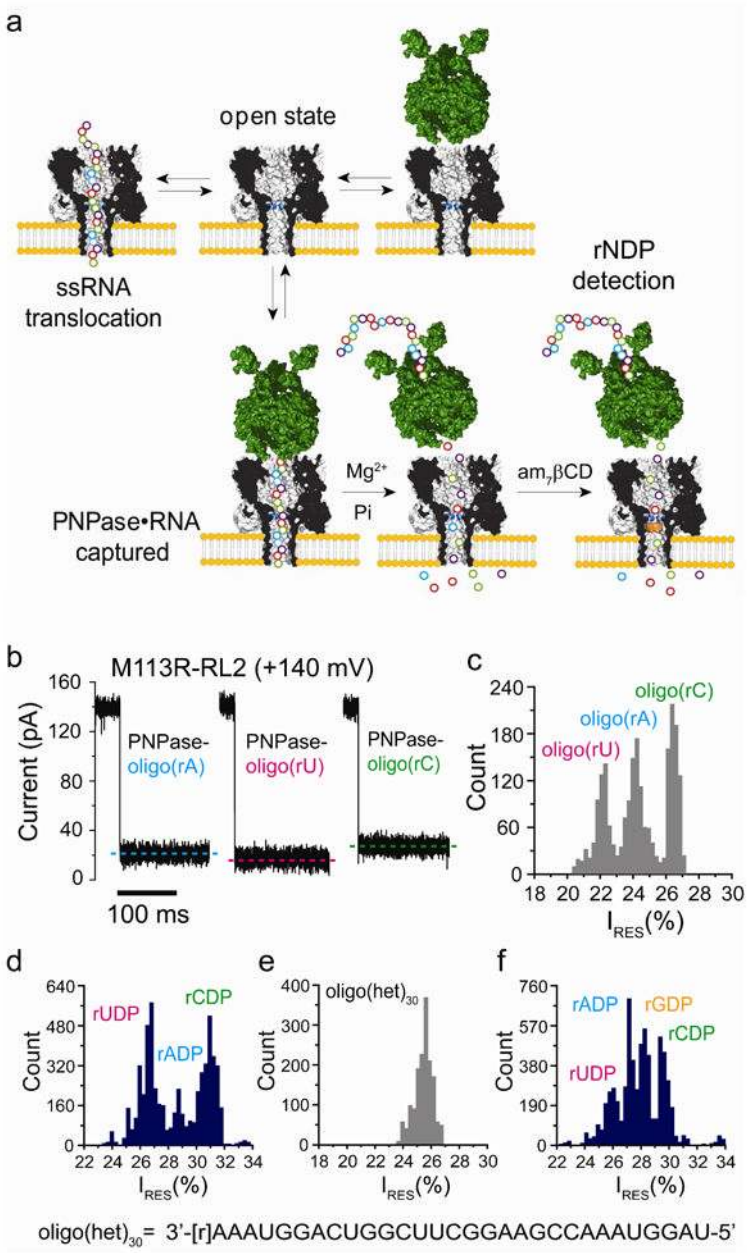

Figure 4.

Detection of nucleosides diphosphates cleaved from ssRNA by PNPase. (a) Upon the addition of ssRNA, without the enzyme, current blockades are caused by brief ssRNA translocation events. In the presence of PNPase, additional blockades with longer residence times and/or amplitudes that differ from those of the translocation events are observed when PNPase•RNA complexes are captured. After the addition of Mg^{2+} and inorganic phosphate (P_i), followed by the addition of $_7$βCD (*trans*), cleaved nucleotides are detected through their interactions with the CD adapter. (b) Current traces for the capture of homopolymeric ssRNAs bound to PNPase by the αHL M113R-RL2 pore at +140 mV. (c) Histogram of the residual current levels ($I_{RES\%}$) after capture of homopolymers ssRNAs bound to PNPase by the αHL M113R-RL2 pore at +140 mV. (d) Histogram of the residual current levels ($I_{RES\%}$) for the rNDP binding events with am$_7$βCD (trans). The rNDPs were cleaved by PNPase

from the RNA homopolymers, oligo(rA)$_{30}$, oligo(rC)$_{30}$ and oligo(rU)$_{30}$. e) Histogram of the residual current levels ($I_{RES\%}$) after capture of a PNPase-bound hetero-oligomeric ssRNA (oligo(het)$_{30}$: 3′-[r]AAAUGGACUGGCUUCGGAAGCCAAAUGGAU-5′) inside the αHL M113R-RL2 pore at +120 mV. (f) Histogram of the residual current levels ($I_{RES\%}$) for rNDP binding events in the presence of am$_7$β CD(trans). The rNDPs were cleaved by PNPase from the hetero-oligomeric ssRNA, oligo(het)$_{30}$(Figure S11).

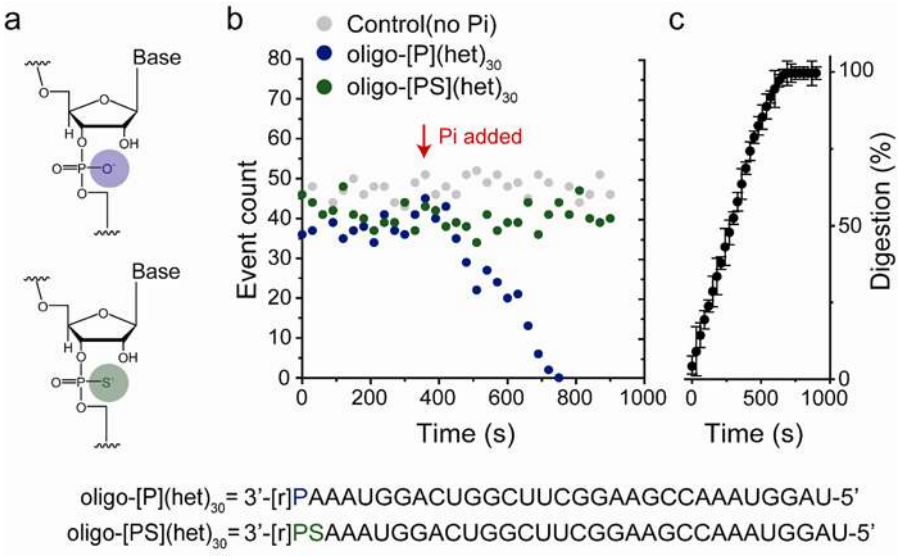

Figure 5.

Monitoring PNPase digestion of ssRNA with a nanopore. (a) Chemical structures of the phosphodiester linkage in oligo-[P](het)$_{30}$ (top, blue circle) and the phosphorothioate linkage in oligo-[PS](het)$_{30}$ (bottom, green circle), which is not hydrolyzed by PNPase. (*Below*) Sequences of the hetero-oligomeric oligonucleotides. (b) The PNPase bound oligo-[P](het)$_{30}$ ssRNA capture rate in the M113R-RL2 nanopore as a function of time. After the addition of 10 mM P_i (red arrow), the event rate sharply declines for the PNPase-oligo-[P](het)$_{30}$. In contrast, the event rate is maintained for PNPase-oligo-[PS](het)$_{30}$. (c) Time course for oligo-[P](het)$_{30}$ ssRNA digestion by PNPase (n = 3). The plot was constructed by collecting capture events in a 30 s segment (from t= 0 s to 900 s), in the presence of P_i and Mg^{2+}.

Table 1

Comparsion of kinetic parameters for rNDP identification. Comparison of the kinetic parameters of optimal nucleoside diphosphate binding to $am_7\beta CD$ and $gu_7\beta CD$ within the M113R-RL2 αHL mutant pore at pH 6.0 (+120 mV) and to the covalent α HL-$(N139Q)_6(N139Q/L135C)_1$.am_6-$amPDP_1\beta CD$ pore at pH 7.5 (+160 mV). Values of k_{off} were determined by using $k_{off} = 1/\tau_{off}$, where τ_{off} is the mean dwell time of each rNDP in the pore. I_O and $I_{RES\%}$ values are mean values (±S.D.) taken from Gaussian fits to event histograms. $I_{RES\%} = (I_{RES}/I_O) \times 100$. $\Delta I_{RES\%}{}^{OVERALL}$ is the difference in residual current between the two most widely separated current peaks. δ is the product of the successive differences in $I_{RES\%}$ between the four peaks. If any two peaks overlap, then δ is zero.

Nucleotide	M113R-RL2 (+120 mV)						αHL-$(N139Q)_6(N139Q/L1\ 35C)_1$.$am_6$-$amPDP_1$-βCD (+160 mV)		
	$am_7\beta CD$			$gu_7\beta CD$					
	τ_{off} (ms)	k_{off} (s^{-1})	I_{RES} (%)	τ_{off} (ms)	k_{off} (s^{-1})	I_{RES} (%)	τ_{off} (ms)	k_{off} (s^{-1})	I_{RES} (%)
rGDP	11.0 ±1.0	91.0 ±4.0	23.1 ±1.4	16.0 ±1.2	43.0 ±6.0	25.6 ±1.2	26.0 ±2.0	39.0 ±1.0	28.0 ±0.2
rADP	20.0 ±1.6	50.0 ±6.0	21.9 ±0.8	21.0 ±1.1	46.0 ±6.0	23.0 ±1.2	22.0 ±2.0	46.0 ±1.0	29.4 ±0.3
rCDP	16.0 ±2.0	63.0 ±2.0	24.1 ±1.2	17.0 ±1.2	42.0 ±8.0	26.4 ±1.6	23.0 ±2.0	44.0 ±1.0	31.7 ±0.3
rUDP	9.0 ±1.0	111.0 ±6.0	20.7 ±1.0	11.0 ±1.0	49.0 ±6.0	22.1 ±2.0	18.0 ±3.0	56.0 ±1.0	32.7 ±0.3
$\Delta_{IRES}{}^{OVERALL}$(%)	3.4 ±0.3			4.3 ±0.4			4.7 ±0.3		
δ	1.4 ±0.6			1.9 ±0.4			3.2 ±1.0		